Towards engineering the design of internal interfaces through interfacial segregation in steels

Mainak Saha[1,2]

[1] Department of Metallurgical and Materials Engineering, National Institute of Technology Durgapur-713209, West Bengal, India

[2]Department of Metallurgical and Materials Engineering, Indian Institute of Technology Madras, Chennai-600036, India

Corresponding authors: Mainak Saha

Email address (es): mainaksaha1995@gmail.com

Phone number: +918017457062

ORCID: Mainak Saha: 0000-0001-8979-457x

Abstract

A range of phenomena, including changes in interface structure, mobility, cohesion, etc., are brought on by soluble decoration at grain boundaries (GB). Recent experimental studies on the interfacial segregation of steels are based on the microstructural characterization of the steels employing two correlative methods, namely Transmission Electron Microscopy-Atom Probe Tomography (APT) and Electron Backscatter Diffraction-APT. The current study aims to address the typical adsorption isotherms used for assessing interfacial segregation and provide an overview of the current status of experimental research in the area of GB segregation in steels in light of the increased interest in this field. An emphasis on the experimental challenges related to comprehending GB segregation in steels has also been placed on the areas where an understanding of GB segregation may be useful.

Keywords: Grain boundaries, solute decoration, correlative microscopy, cohesive strength

1. Introduction

Grain boundaries (GBs) are planar (2D) defects that affect a variety of properties, including tensile strength, in polycrystalline metallic materials. corrosion resistance, endurance to hydrogen (H) attack, thermal and electrical conductivity, etc. [1]–[5]. A GB may also function as a source and sink for vacancies and dislocations since it is a region of partial atomic disorder with specified structure and direction. [6]–[9]. They also have five macroscopic degrees of freedom (DOFs), including misorientation axis and angle. [10]–[15]. A GB's structure is determined by the five DOFs [16]–[19]. The energy of a GB, often referred to as GB energy, is strongly impacted by GB structure and by the chemistry close to GBs [17], [18], [20]-[24].

The reduction of GB energy is what motivates solute decoration at GBs [25]–[27]. As compared to random high-angle GBs (RHAGBs) (with high GB energies), special high-angle GBs (SHAGBs) with low GB energies have been claimed to have considerably higher resistance to corrosion, crack propagation, H diffusion, GB sliding, etc. [28]-[31]. As a result of these observations, GB engineering (GBE), which is based on substituting SHAGBs for RHAGBs in order to optimise the properties (of polycrystalline materials), has evolved. [32]–[37]. However, it is important to take into account the influence of preferential segregation of various elements (with varying concentrations) at GBs [2], [38]-[42]. This is crucial since the majority of GB features, including fracture toughness, electrical and thermal properties, H embrittlement, resistance to dislocation pile-up, etc., are affected by segregation-induced changes [2], [43]. GB segregation engineering (GBSE) is the term used to describe this modification of the GB structure [2]. Co-segregation, the coefficient of segregation, and other thermodynamic and kinetic variables, like deformation-induced GB phase evolution, are all linked to GBSE [2], [44]–[46]. This implies that solute decorating at GBs is significantly impacted by time [2] in addition to thermomechanical treatment. Additionally, elemental segregation is used by GBSE as a site-specific manipulation technique that optimises a particular GB structure's composition and attributes [2].

Additionally, polycrystalline metallic materials' strengths may be decreased or increased by GBs [1]. Due to the high stress concentration along GBs, the majority of metallic materials in service are likely to fail from an intergranular fracture by void nucleation and propagation [47]. The most typical explanation for such a failure is predominant GB embrittlement caused by plastic strains along GBs not being accommodated in the presence of segregating solute species [48], [49]. Metallic materials have "impaired plasticity" as a result of this embrittlement-assisted failure [50]. The embrittlement that results from the segregation of H at various GBs in steels is a fairly prevalent example of this phenomena [2], [51]. The accommodation of plastic strains along GBs, particularly in the presence of solute segregation, has instead been the subject of several papers on the strengthening of GBs (in metallic materials) [40], [52]–[54]. Thus, creating metallic materials with great overall toughness is the main goal. The former remark frequently holds true in the context of steels, which are the foundation of the world economy. To put it another way, designing high-performance steels may make use of solute ornamentation at internal interfaces [2]. The objective of the current review paper is to discuss typical thermodynamic methods for estimating the degree of interfacial segregation and to highlight the current experimental research in the area of GB segregation in steels. The

potential applications of knowledge of GB segregation have also been addressed. Additionally, the solute segregation perspective has been used to briefly address the experimental difficulties related to GB research.

2. Relevant topics

2.1 Theoretical approaches towards quantifying interfacial segregation

According to certain reports, the solute concentration at GB is up to several orders of magnitude greater than the solubility (of the solutes) in the interior of the grain [1], [2], [48], [55]-[57]. According to Raabe et al. [2], bulk solubility (the solubility of a specific solute inside a grain) can be used as a rough indicator of a solute's propensity for preferential segregation at GBs. In other words, the higher the solute enrichment factor (β_i) of the solute at the GB, the smaller the bulk solubility, and the greater the inclination of the solute species towards GB segregation [2]. The fluctuation of β_i as a function of the maximum solubility of several solutes in the α-Fe matrix is depicted in Fig. 1.

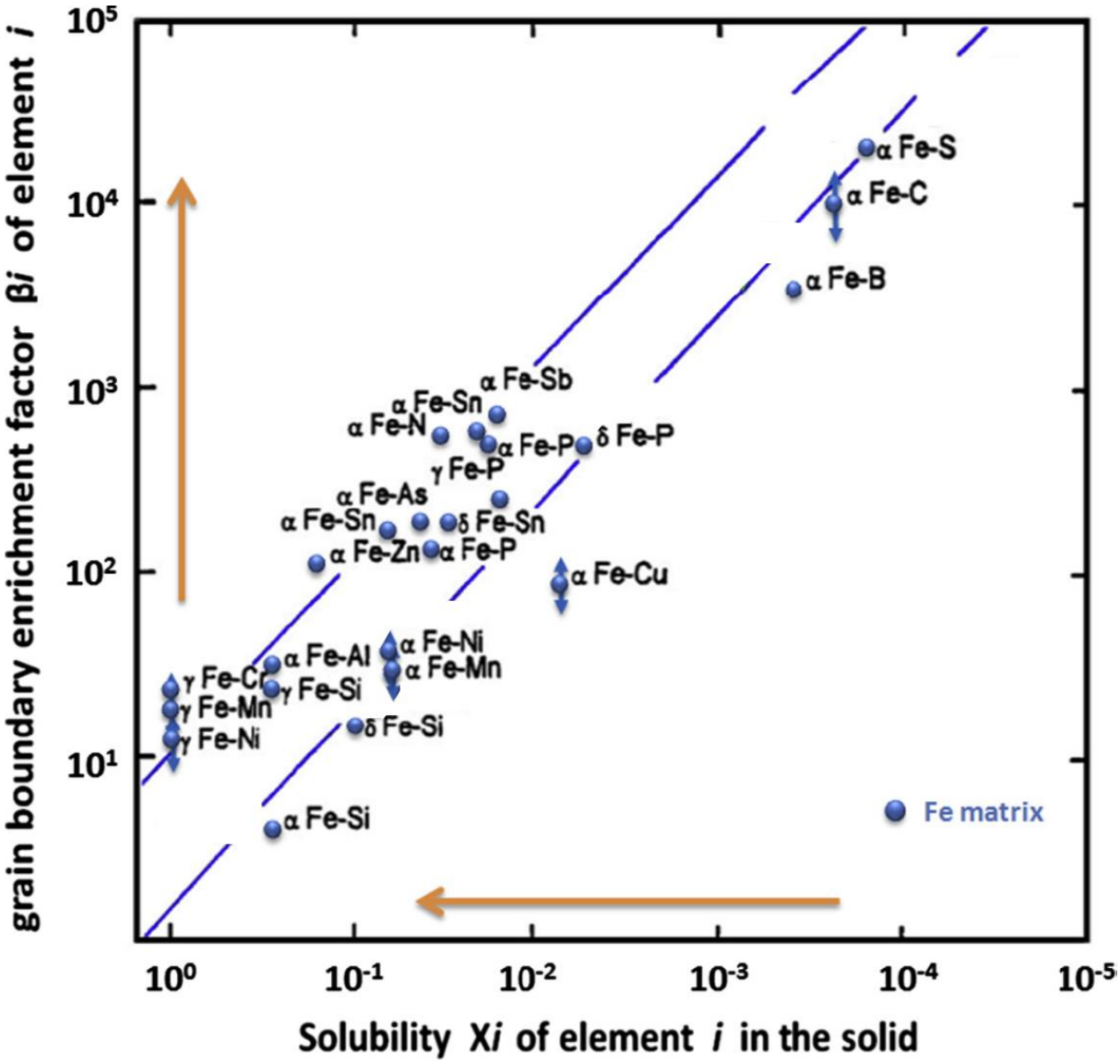

Fig. 1 Variation of β_i in relation to the maximum solubility of several solutes in the α-Fe matrix, as in Ref. [2]. The data points in this plot can be utilised to find suitable solute species that have a propensity to segregate into GBs.

Additionally, the thermodynamics involved in GB segregation may be expressed in terms of the Gibbs adsorption isotherm and is a near analogue of monolayer gas adsorption at solid surfaces [16], [58]. This isotherm can be used to determine the excess concentration of a specific solute species at a GB, also known as GB excess: [16]

$$\Gamma_i = -\left(\frac{1}{RT}\right)\left(\frac{d\gamma_{GB}}{dx_i}\right)_{V,T} \quad (1)$$

Where: R is the universal gas constant (8.314 J/molK), x_i is the molar concentration of the element (solute) i in the bulk (or grain interior), $d\gamma_{GB}$ is the change in GB energy upon

segregation at a certain temperature T and volume V, and T is the absolute temperature (in K). [16]. Theoretically, Γ_i can be calculated by measuring $d\gamma_{GB}$ as a logarithmic function of dx_i. The other type of Gibbs adsorption isotherm, which connects $d\gamma_{GB}$ with Γ_i and changes in the chemical potential of solute i ($d\mu_i$), is frequently utilised in the context of GB segregation. It is written as: [58]

$$d\gamma_{GB} = -\sum_i \Gamma_i d\mu_i \quad (2)$$

The Gibbs adsorption isotherm is based on a crude method for estimating GB segregation from a thermodynamic perspective. The aforementioned isotherm, however, cannot be used to assess GB segregation as a function of bulk concentration and temperature [59], [60]. Since it quantifies GB segregation by balancing both the adsorption and desorption rates of solute species at a GB, the Langmuir-McLean isotherm has been extensively employed in this context [60]. As of [60], this isotherm is given as:

$$\frac{{x_i}^{GB}}{({x_i}^{GB,0} - {x_i}^{GB})} = \frac{{x_i}^{B}}{(1 - {x_i}^{B})} \exp\left(-\frac{\Delta G_i^{GB}}{RT}\right) \quad (3)$$

where ${x_i}^{GB}$ denotes the molar concentration of the solute i at GB, ${x_i}^{GB,0}$ denotes the solubility limit of the solute i at GB, ${x_i}^{B}$ denotes the molar fraction of the solute i in the bulk of the grain, and ΔG_i^{GB} denotes the Gibbs molar free energy of segregation of the solute i [60]. Equation (3) can be made simpler by assuming that the system is diluted as follows: [60]

$$\beta_i = \frac{{x_i}^{GB}}{{x_i}^{B}} = \exp\left(-\frac{\Delta G_i^{GB}}{RT}\right) \quad (4)$$

The value of ΔG_i^{GB} is typically unknown. Equations (3) and (4) suggest that GB segregation occurs when $\Delta G_i^{GB} < 0$, and that this tendency of solute to segregate at GBs decreases with increasing temperature [60]. The main drawback of the Langmuir-McLean isotherm is that, in contrast to the Gibbs adsorption isotherm [2], [61], it does not take GB energy into account when quantifying GB segregation. Additionally, this isotherm presupposes that, in the event of several decorating solutes, dynamic equilibrium is reached between the segregating solute species and that, at GBs, solute decoration is restricted to a single monolayer [60]. However, neither of the aforementioned isotherms takes into account the interaction between segregating solute species at GBs and instead treats GB as a separate phase with characteristics that are distinct from those in the interior of the grain [2].

In α-Fe based alloys, the phenomena of entropy-dominated GB segregation has recently been reported for low solute concentration at various SHAGBs and RHAGBs [62]. The notion that the phenomena of GB segregation is only governed by the enthalpy of segregation (ΔH_i, for solute i) and not by the entropy of segregation (ΔS_i) has reportedly been linked to the main restriction of the Langmuir-McLean isotherm [62], [63]. Furthermore, it has been theoretically demonstrated that, particularly at homologous temperatures > $0.4T_m$ (T_m: melting points (in K)), entropy-dominated segregation phenomena is prevalent for solutes with poor solid solubility in a given matrix (solvent). Sb and Sn are the two often segregating species with low solid solubility in the context of α-Fe based matrices [62], [64]. At temperatures below 450°C, these elements have been shown to exhibit dominant entropy-dominated GB segregation [62].

Lejcek and Hoffmann [65]–[67] have demonstrated that solubility limits for various solute atoms at various GBs vary with GB character in α-Fe based on GB segregation maps at various temperatures. Therefore, it may be inferred that GB segregation diagrams help us comprehend how solutes segregate in dilute binary systems. To determine the degree of solute segregation at various GBs, it is always more advantageous to understand GB segregation in multicomponent alloys where mutual interactions and site competition both concurrently play a significant role [50], [67]-[70]. When this occurs, β_i is unable to accurately forecast how much solute segregation will occur at GBs [65], [68], [71]–[77]. For a ternary system with matrix M and the other solute j, according to Guttmann [78]-[80], ΔH_i is given by:

$$\Delta H_i = \Delta H_i^0 - 2\alpha_{Mi}(x_i^{GB} - x_i) + \alpha_{ij}(x_j^{GB} - x_j) \quad (5)$$

where x_i^{GB}, x_j^{GB}, and x_i, x_j are the GB and bulk mole fractions respectively of two solutes, i and j. ΔH_i is influenced by the chemical reactions taking place between the constituents, namely the binary interaction with the Fowler interaction coefficient α_{Mi} and the ternary interaction coefficient $\alpha_{ij}^{'}$ with the other solute species [81]. Even for a multicomponent system, ΔH_i^0 denotes the enthalpy of segregation for the diluted binary system M-i and is temperature and composition independent [80]. As a result, ΔH_i^0 in equation (5) is a separate feature of the segregation of solute i in matrix M [81]. As a result, it may be acceptable to claim that a more fundamental thermodynamic parameter, such as ΔH_i, better describes a solute's inclination to segregate at GBs compared to β_i in multicomponent systems.

2.2. Characterising GB segregation in steels

2.2.1 Common techniques for the characterisation of GB segregation

A number of characterisation techniques have been used to investigate GB segregation such as Auger Electron Spectroscopy (AES), Transmission Electron Microscopy (TEM), Scanning Transmission Electron Microscopy (STEM), Electron Backscatter Diffraction (EBSD), Transmission Kikuchi Diffraction (TKD), Electron Energy Loss Spectroscopy (EELS), Field Ion Microscopy (FIM), Secondary Ion Mass Spectroscopy (SIMS) and Atom Probe Tomography (APT). When employed singly for characterising GB segregation, each of these methods has a number of drawbacks, mainly the absence of crystallographic information and high spatial resolution GB segregation data [2]. Furthermore, because GB segregation occurs on an atomic scale, it is difficult to gather information about GB segregation that is accurate, statistically significant, and reproducible all at once [2]. The current disparity between the theoretical and experimental approaches to tackling GB segregation has been emphasised by Wynblatt and Chatain [82].

Correlative microscopy, which enables the simultaneous determination of both structural and chemical information from an area surrounding a solute-decorated GB, is one of the recently developed approaches for characterising GB segregation. The two correlative characterisation approaches used (to date) for the assessment of GB segregation in steels are based on the direct lattice reconstruction from a provided APT data of solute-decorated GBs (Correlative TEM-APT and EBSD-APT approach) [2], [83]-[85]. Additionally, a variety of factors can affect the GB segregation information discovered using electron microscopy methods (such TEM and EBSD). First, the angular resolution of the employed electron microscopy method needs to be considered. Depending on the instrument and analysis software utilised, using the TEM-based nanobeam diffraction approach, it is possible to achieve an angular resolution of 1° as opposed to the (1-3°) attained using the EBSD technique [86]. Second, using the Focused Ion Beam (FIB)-based liftout process in a scanning electron microscope (SEM) to produce APT tips (including the GB region) is fraught with ambiguity [2], [87]. Prior orientation mapping on the APT tips using TEM and/or FIM techniques was previously used to alleviate this issue. In addition to the restricted range of view, employing these approaches to get exact orientation information (from APT tips) calls for a high level of competence. The field of view of the TKD technique is greater than that of the TEM and FIM procedures [88, [89]. Additionally, TKD is significantly simpler to use than TEM and/or FIM procedures for getting orientation information [90]. The impact of projection and lens effects on the allocation of atoms to a certain GB [91]–[93] is one of APT's limitations. The lens effect is connected to field evaporation at solute-decorated GBs and causes inaccuracies in the positioning of field

evaporated atoms, while the projection effect is based on the magnetic field around the APT tip [91].

2.3 Experimental investigations towards understanding GB segregation in steels

2.3.1 Conventional methodology

Grabke et al. [94] investigated the segregation of Ti, Nb, Mo, and V and associated carbides at RHAGBs in Fe-P based ternary and quaternary alloys (bulk composition is specified in Ref. [94]) using FIM, APT, and AES techniques. In Fe-Ti-P ternary alloys, Ti and Nb addition was shown to inhibit the segregation of P at GBs (via the creation of Ti and Nb-based phosphides) [94]. However, it was noted that neither Mo nor V had an impact on propensity of P towards segregation [94]. GB segregation of P in Fe-Nb-C-P and Fe-Ti-C-P quaternary alloys increases with C concentration up to the point at which NbC precipitates form [94]. Using AES, Christien et al. [95] have demonstrated a linear relationship between the concentration of P isolated at GBs in a 17-4PH martensitic stainless steel and the intergranular grooves created during metallographic etching. The segregation of C and N atoms at various GBs in Fe-0.006C-0.001N-0.04Al (C60) and Fe-0.005C-0.0054N-0.04Al (N60) (wt.%) ferritic steels has been studied by Takahashi et al. [96] using APT. It was noted that, based on the observations, C segregates at RHAGBs in C60 while N segregates at RHAGBs in N60 [96]. However, it was shown that N in N60 had a lower tendency to segregate than C in C60 [96]. Additionally, it was noted that the segregation of C atoms at RHAGBs (in C60) and not the segregation of N atoms at RHAGBs (in N60) had an impact on the Hall-Petch coefficient of ferrite grains [96].

Rosa et al. [97] used nano-SIMS and APT techniques to examine the effects of B addition on high strength Fe-0.34C-2.45Mn-0.0100B-0.03Ti (at.%) steel (with a single-phase austenitic structure). The segregation of B at RHAGB is caused by the dissolution of boride (Fe_2B and $M_{23}(B,C)_6$) precipitates in grain interior [97]. Additionally, it was noted that the degree of B segregation at austenite GBs increased with temperature [97]. B segregation at austenite GBs was claimed to follow the Langmuir-McLean adsorption isotherm [97], despite the fact that this goes against the thermodynamically supported trend of decreased solute segregation with increasing temperature. B segregation at austenite GBs was claimed to follow the Langmuir-McLean adsorption isotherm [97], despite the fact that this goes against the thermodynamically supported trend of decreased solute segregation with increasing temperature. The enthalpy of dissolution (ΔH_{diss}) of borides and the ΔH_i of B (at austenite GB) were computed based on this isotherm to be greater (by 51% and 9.4%, respectively) than the corresponding values (of ΔH_i

and ΔH_{diss}) published in the earlier literatures [98]-[100]. Using APT, AES, and fractography techniques, Fedotova et al. [101] examined irradiation-induced GB segregation of P, Mn, Ni, and Si at RHAGBs in Fe-(0.04-0.07)C-(1.6-1.89)Ni-(0.006-0.01)P (wt.%) reactor pressure vessel steels. According to reports, the degree of these elements' segregation (at RHAGBs) increased with the bulk concentration [101]. Additionally, inter-granular fracturing was seen to be promoted by P segregation at RHAGB [101]. Similar P tendencies have been seen in neutron-irradiated AISI 304 austenitic stainless steel [103], [104], and Fe-(0.083-0.19)C-(0.26-0.38)Si-(1.22-1.41)Mn-(0.007-0.012)P (wt.%) reactor pressure vessel steels.

Using the aberration-corrected STEM-EELS technique, Shigesato et al. [105] studied the non-equilibrium segregation of B at austenite RHAGBs in Fe-0.05C-0.5Mo-0.001B (wt.%) steel. Additionally, this work [105] evaluated the effects of specimen thickness, electron beam broadening, and GB plane orientation on the GB segregation of B. The broadening of the B concentration profile was calculated using the Gaussian broadening model [105]. Specimen thickness increases the degree of widening [105]. The widening of the B concentration profile was found to be 10% [105] for specimen thickness of 30 nm. Additionally, it was noted that the B concentration profile was asymmetric for GB plane inclination angles greater than 1.5° [105]. In a duplex medium Mn steel (composition: Fe-11.7Mn-2.9Al-0.064C (wt.%)), Ma et al. [106] have demonstrated that segregation of C at ferrite/austenite interphase boundary (IB) leads to an increase in the energy barrier for dislocation emission from RHAGBs, resulting in discontinuous yielding of the material at room temperature. It has been suggested that the discontinuous yielding phenomena is influenced by C-decoration at the aforementioned IB in conjunction with dislocation nucleation and subsequent multiplication [106]. Additionally, contrary to earlier results [107]–[109], it was shown that Gibbs and Langmuir-McLean adsorption isotherms are not responsible for the segregation of solutes at IBs.

2.3.2 Correlative methodology

TEM-APT methodology

Herbig et al. [86] have characterised C-decorated GBs in a nanocrystalline cold-drawn pearlitic steel (composition: Fe-4.40C-0.30Mn-0.39Si-0.21Cr (at.%)) using correlative TEM-APT methodology and reported the variation of C excess (obtained using APT) as a function of GB misorientation angle for coherent Σ5 and both coherent and incoherent Σ3 GBs (Fig. 2). The overlay of C decoration at various GBs in an APT needle is depicted in Fig. 2(a). The fluctuation of C excess as a function of GB misorientation angle is depicted in Fig. 2(b). C-

excess was discovered to be significantly larger for incoherent Σ3 GBs than for coherent Σ5 and Σ3 GBs [86]. Additionally, it was determined that the presence of misfit dislocations, which are likewise accountable for the significant C-excess at the aforementioned GB (Fig. 2(b)), was the cause of the deviation from the optimum 60° misorientation (for incoherent Σ3 GBs) [86]. For the aforementioned GBs, it was also shown that the C excess vs. GB misorientation angle plot had a strong association with the GB energy vs. misorientation angle plot [86]. The similar methodology was utilised by Abramova et al. [110] to demonstrate how Mo, Si, and Cr segregation at austenitic RHAGB causes GB strengthening in ultra-fine grained AISI 316 austenitic stainless steel. Han et al. [111] have reported using the aforementioned technique that delamination is significantly influenced by competitive segregation of C and P (at RHAGBs) in the context of Fe-1.62Mn-0.18Si (wt.%) ferritic steel. Additionally, it was noted that RHAGBs with high P and low C content induce delamination cracks, whereas RHAGBs with low P and high C content were shown to be resistant to delamination cracking [111].

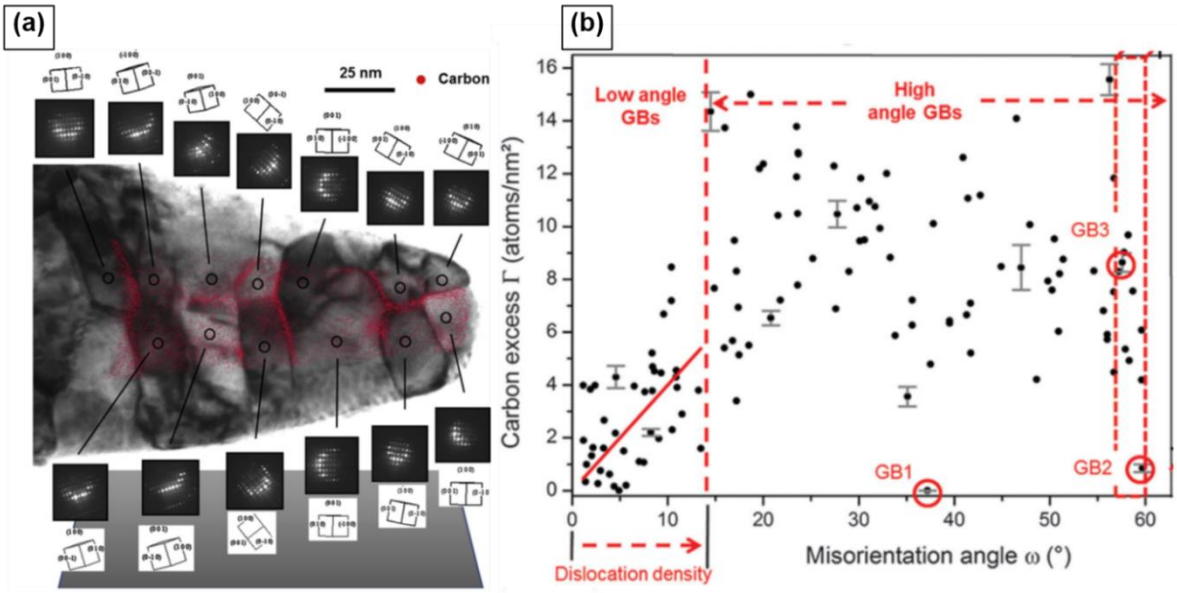

Fig. 2 Correlative TEM-APT analysis for cold drawn pearlitic steel with the following composition: Fe-4.40C-0.30Mn-0.39Si-0.21Cr: APT needle prepared using FIB-based liftout approach (a) Overlay of C decoration at various GBs (b) Variation of C excess as a function of GB misorientation angle [86].

EBSD-APT methodology

This methodology was utilised by Kuzmina et al. [112] to demonstrate how Mn segregation causes martensite RHAGBs in Fe-9Mn-0.05C (wt.%) steel to become embrittled at 450°C. In

that situation, it was reported that the addition of 0.0027 wt.% B strengthened the GB and prevented the segregation of Mn at martensite RHAGB by encouraging martensite to austenite reversion during a protracted holding period of around 336 hours at 450°C [112]. Benzing et al. [113] observed a similar finding in relation to Fe-12Mn-3Al-0.05C (wt%) steel. This methodology was used by Ravi et al. [114] to investigate the effects of C segregation in Fe-0.2C-3Mn-2Si (wt.%) bainitic steel. They found that C segregation at austenite RHAGBs facilitates austenitic to bainitic transformation during isothermal holding at bainitic transformation temperature (400°C, in this case).

The segregation of B, C, P, Si, and Cu at an FCC RHAGB and coherent Σ3 annealing twin boundaries in Fe-28Mn-0.3C (wt.%) twinning-induced plasticity (TWIP) steel was characterised by Herbig et al. [115] using the same method (Fig. 3). Image quality (IQ)+GB map based on EBSD is shown in Fig. 3(a). The APT-based 3D concentration profiles of B, C, Si, P, Mn, and Cu at the two GBs highlighted in Fig. 3(a) are shown in Figs. 3(b) and 3(c). According to Figs. 3(b and c), the degree of Mn segregation was found to be essentially the same for both RHAGB and at Σ3 GB. According to Figs. 3(b and c) [115], B and P were shown to segregate substantially more strongly at RHAGB than at coherent Σ3 annealing twin boundaries. This was explained by the fact that RHAGB has a higher GB energy than coherent Σ3 GB [115]. According to a study, adding C atoms to RHAGB (Fig. 3(b)) increased the local stacking fault energy (SFE), which in turn caused high resolved shear stress for mechanical twinning (at RHAGB) [115]. On the other hand, it was noted that C depletion (at Σ3 GB; Fig. 3(c)) decreased the local SFE and caused the development of the ε-martensite (HCP) phase at austenite Σ3 boundaries [115]. Additionally, it was examined whether elements (B, C, P, and Si) preferentially segregated at deformation and/or annealing twins in a deformed Fe-22Mn-0.6C (wt.%) TWIP steel [115]. Although they have identical crystal structures, deformation twins exhibit a significantly reduced propensity to develop C atom decorating than annealing twins [115]. The extremely poor mobility of C atoms during the production of deformation twins at room temperature may be the reason for this tendency of deformation twins [115].

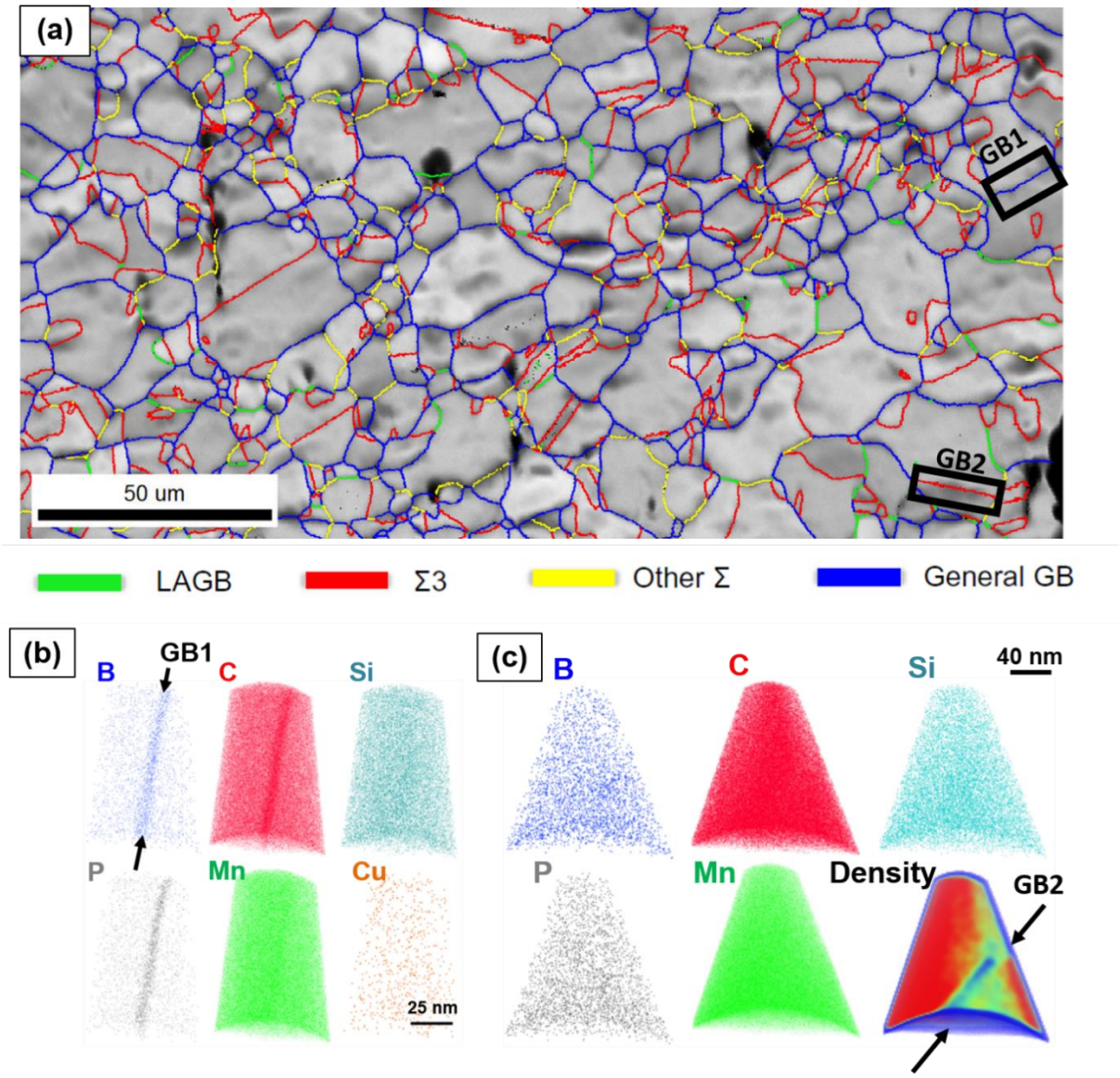

Fig. 3 Correlative EBSD-APT analysis for Fe–28Mn–0.3C (wt.%) TWIP steel: **(a)** EBSD-based IQ+GB map showing the two GBs: GB1 and GB2 (enclosed in black outlined rectangular boxes) analysed using APT, APT-based 3D elemental maps for different elements in **(b)** GB1 and **(c)** GB2. In part **(a),** LAGB abbreviates for low-angle grain boundary and general GB refers to RHAGB. To the bottom right of part **(c)**, Density map (of Fe) shows the position of GB2 [115].

Araki et al. [116] developed a systematic correlation between the critical shear stress for dislocation emission from GB and the concentration of C at (a) grain interior and (b) RHAGB in Fe-50C (ppm) ferritic steel using the aforementioned correlative methodology in conjunction with the nanoindentation technique. Based on this research, it was found that (i) dislocation nucleation and multiplication occur much more readily at RHAGB than in grain interiors due to the high frequency of "pop-ins" (in load-displacement curves) at RHAGB, and (ii) pinning

of dislocations by C atoms segregated at RHAGB results in a high critical shear stress for emission of dislocations from RHAGB, leading to GB strengthening [116]. Additionally, before the commencement of "pop-in events" in nanoindentation-based load-displacement curves, the critical shear stress necessary for dislocation emission from RHAGB was estimated using Hertz contact theory, taking into account elastic contact between the nanoindenter and the sample surface [116]. The extant literature on the use of TEM-APT and EBSD-APT based correlative approaches to characterise GB segregation in steels is compiled in Table 1.

Table. 1 A summary of reports based on correlative approach towards characterising GB segregation in steels (till date) [19].

Correlative approach	Steel composition (or grade)	Segregating solute species	Type of GB	Reference
TEM-APT	Fe–4.40C–0.30Mn–0.39Si–0.21Cr (at. %)	C	Coherent Σ5, coherent and incoherent Σ3	[86]
	AISI 316	Mo, Si, Cr	RHAGB	[110]
	Fe-1.62Mn-0.18Si (wt.%)	C, P	RHAGB	[111]
EBSD-APT	Fe-9Mn-0.05C (wt.%)	Mn	RHAGB	[112]
	Fe-12Mn-3Al-0.05C (wt.%)	C, Mn	RHAGB, IB, triple junctions	[113]
	Fe–0.2C–3Mn–2Si (wt.%)	C	RHAGB	[114]
	Fe–28Mn–0.3C (wt.%)	B, C, P, Si	coherent Σ3	[115]
	Fe–22Mn–0.6C (wt.%)	B, C, P, Si	Σ3 deformation twins	[115]
	Fe-50C (ppm)	C	RHAGB	[116]

2.4. Towards utilising GB segregation: Examples

2.4.1 Alloy design

One use of GB segregation in the context of steel design is to stabilise nano-sized grains by lowering the overall GB energy through solute decorating at GBs. As an illustration,

discontinuous grain growth (caused by high GB energy) is a frequent occurrence that has been seen in a variety of materials, particularly steels. In that situation, GB segregation is beneficial in two different ways. It first lowers the GB energy and then the capillary force linked to the competitive growth of two adjacent grains. Second, selecting suitable solutes (for decorating at GBs) improves GB cohesive strength. According to Yuan et al. [117], the segregation of C at martensite GBs increases the ultimate tensile strength and total elongation (by around 233.33% and 53%, respectively) in Fe-13.6 Cr-0.44 C (wt.%) martensitic steel. This was explained by the segregation of C at martensitic GBs, which promotes the transition from the martensite to austenite phase [117]. In Fe-3.66C-0.48Mn-0.39Si-0.01P-0.01S (at.%) pearlitic steel, Li et al. [118] found a direct association between the amount of tensile deformation and the concentration of segregated C at ferrite RHAGBs. Additionally, in hypereutectoid Fe-4.40C-0.30Mn-0.39Si-0.21Cr-0.003Cu-0.01P-0.01S (at.%) pearlitic steel, a similar correlation for the situation of C separated at ferrite sub-grain (or, low angle) boundaries has been shown [119], [120].

Designing steels with resistance to H embrittlement (HE) is another application for which knowledge of GB segregation may be useful. One of the most frequent issues with automotive grade steels is HE [121]–[129]. Being the smallest atom (atomic radius 0.037 nm), H easily diffuses into materials (particularly steels) and causes engineering components to break catastrophically and without precedent while in use [122]. In addition, it is difficult to map the precise location of H in a material due to the extraordinarily high atomic mobility of H (caused by the small atomic radius). As a result, it is very difficult to validate a number of existing tactics (developed for steels such as the addition of carbides). Chen et al. [124] recently created a deuterium charge based cryo-transfer process to locate H atoms separated at various GBs in Fe-0.23C-0.92Mn-0.24Si-0.049Nb (wt.%) steel using characterisation techniques like TEM, TKD, and cryo-APT. Two different forms of microstructures: completely martensitic and wholly ferritic were examined using this technique [124]. Deuterium was shown to segregate at the incoherent interfaces between NbC and ferrite in the completely ferritic microstructure and between NbC and martensite laths in the completely martensitic microstructure [124]. This was the first observation made through experiment regarding a carbide's capacity to hold hydrogen atoms. C was also seen to significantly segregate at low-angle lath boundaries in the case of the fully martensitic microstructure [124]. C was shown to be substantially segregated at ferrite RHAGBs in the case of the completely ferritic microstructure [124]. Additionally, it has been noted that the GB misorientation angle in ferrite RHAGBs affects the GB segregation

tendency for C atoms [124]. Both C and H atom segregation (at various GBs) were observed in both microstructures at the same time [124]. Despite the great affinity of C for the H atom, it was reported that H was trapped at GBs [124].

2.4.2 Stress and segregation-induced phase transformation at a GB

According to Raabe et al. [2], local elastic stresses and solute decoration (at GBs) can be used to encourage localised phase change. This is frequently noticed when martensite to austenite reversion occurs at martensite GBs. The energy of martensite GBs has an impact on the reversion phenomenon [130]. Additionally, it has been noted that the transformed region (at GBs) can accommodate localised elastic stresses, leading to a localised transformation induced plasticity (TRIP) effect at the transformed austenite GBs, which facilitates additional phase change [120], [130]. The shape of the martensite phase has a significant impact on the martensite GB energy [49]. For instance, a variety of martensite GBs, such as lath, needle, and packet boundaries, have been described in the literature [2], [119]. Lath boundaries, out of all of these boundaries, are linked to the least amount of GB energy [2], [131]-[134]. According to reports, the aforementioned reversion is a very successful technique for stopping intergranular fracture spread along martensite GBs. However, a variety of criteria have been documented by the current literatures [135]-[138] for the occurrence of this reversion. First, it is necessary to select solute species with a high β_i [138]. Second, at martensite GBs, the solute species must prefer to go through preferred segregation [49]. Third, the solute species must be more likely to segregate at GBs than to form precipitates (for example, many transition elements like Ti, V, Cr, Nb, etc. forming carbides) [49]. Fourth, the separated solute species must lower the temperature at which martensite transforms to austenite [135], [136]. In addition, strengthening at GBs must be facilitated by austenite nucleation at GBs [2], [5] and related localised elastic stresses [137].

2.4.3 Influence of GB segregation on GB cohesive strength

In the past, Seah [48] studied the effects of solute adsorption on interface decohesion in commercially pure α-Fe and initially thought about the differences between two types of boundary separation as influenced by solute adsorption: (i) quasi-equilibrium separation with the chemical potential of the solute maintained uniform throughout the system, and (ii) "rapid" separation in a manner that the excess amount of solute initially residing in the boundary remains at the boundary It has been used as the foundation for a model that theoretically calculates GB cohesive strength using atomic sizes and sublimation enthalpies [139].

Additionally, it has been noted that during fracture, dislocations are released in the vicinity of the crack tip and aid in the plastic deformation of the fracture [140]. Failure can occur at lower stress levels if the GB strengthening tendency is inhibited, which also results in a reduction in the amount of plastic surgery required overall [1]. Thermochemical model, which postulated that GB splits without redistribution of the solute atoms during fracture, was utilised for the theoretical investigation of GB cohesion prior to 1979 [1]. However, Seah [48] provided a streamlined numerical evaluation of the behaviour of embrittlement in α-Fe using a Pair Bonding or quasi-chemical model. According to the Pair Bonding hypothesis, the amount of energy actually needed to break the bonds throughout the GB may be easily calculated by counting the dangling bonds in a given location and summing their energies [48], [141]-[143]. According to the model, in α-Fe matrix, Bi, S, Sb, Se, Sn, and Te will be highly embrittling and will cause intergranular separation when mechanical stress is applied, followed by P, As, Ge, Si, and Cu in decreasing order of effect [2], [48]. N, B, and C are listed in ascending order of their ability to avoid intergranular fracture and, as a result, increase overall ductility in α-Fe, by keeping the GB intact [1], [2], [48].

Gibson and Schuh [142], [144] developed GB segregation and associated cohesion maps to determine whether a specific mixture of solute and solvent species will result in GB embrittlement/strengthening and proposed a Bond-breaking model to calculate the change in GB cohesive energy as a function of equilibrium segregation of solute species in α-Fe. According to this model, the energetic barrier to intergranular cleavage is represented by the following equation: [144]

$$E_{GBCE} = 2\gamma_s - \gamma_{GB} \qquad (6)$$

where γ_s is the surface energy. The temperature and composition of the alloy have a significant impact on both of these energies. For solute species separated at GBs, Hirth and Rice [145] have given a mathematical framework for expressing GB cohesive energy (E_{GBCE}) as a function of Γ_i. This thermodynamic approach is predicated on the idea that solute atom segregation at GBs during intergranular cleavage does not occur [145], [146]. The following is the model: [145]

$$\mathrm{E_{GBCE}}(\Gamma) = \mathrm{E_{GBCE}}(\Gamma = 0) - \int_0^{\Gamma} \left(\mu_{GB}(\Gamma) - \mu_S(\tfrac{\Gamma}{2})\right) d\Gamma \qquad (7)$$

where μ_{GB} and μ_S are, respectively, the chemical potentials at the GB and surface. The integral in equation (7) illustrates how the addition of solutes [145], [147]-[151] alters a pure metal's

E_{GBCE}. However, for multi-element segregation at GBs, there is no focus on the interaction between several solute species. Additionally, equation (7) lacks a factor to take GB energy into consideration.

The degree of solute segregation at GBs and free surfaces (FS) has a significant impact on the cohesive strength of GBs [140]. The amount of binding (or segregation) energy present at GB and FS determines whether a solute prefers to segregate there [140], [146]. For instance, the solute atoms operate as potential GB embrittlers when GB cohesive strength is reduced and GB segregation energy is higher than FS segregation energy [140]. The solute atoms increase the GB cohesive strength when the FS segregation energy is greater than the GB segregation energy [140]. The Rice-Wang Model [134] serves as the foundation for this inference's thermodynamic justification. The effect of substitutional factors (like V and P) on the GB cohesive strength of symmetrical tilt Σ5(210) (θ=53.13°) SHAGBs in α-Fe has been theoretically examined by Rajagopalan et al. [140]. It has been demonstrated that P decreases the GB cohesive strength by about Σ5 GB, but V increases the same value [140]. The proposed theoretical methods for calculating GB cohesive energy as a function of solute decoration at RHAGB in α-Fe are listed in Table 2.

Table 2. Theoretical models on determining GB cohesive energy as a function of solute decoration at RHAGB in α-Fe [19].

Proposed model	**Main feature (or assumption)**	**Reference**
Thermochemical	GB cleavage occurs without solute redistribution.	[47]
Pair Bonding or quasi-chemical	Energy required to break the bonds across a GB may be determined by calculating the number of dangling bonds per unit area and adding their energies.	[48]
Hirth-Rice	Constant chemical potential of the segregating species is maintained during GB cleavage.	[145]
Rice-Wang	GB cleavage occurs without any local stress concentration.	[146]
Bond-breaking	Solute (segregated at a GB) does not undergo diffusion during GB cleavage	[147]

By connecting the thermodynamics of GB segregation in solid solutions with GB character, Silva et al. [152] have developed a model for associating GB segregation with intergranular embrittlement and GB phase nucleation. Through research using Atom Probe Tomography (APT) in Fe-Mn binary alloys, the proposed model was experimentally validated [152]. In the case of Fe-Mn alloys, it has been demonstrated that an increase in solute concentration at RHAGBs (BCC RHAGBs) causes an increase in ΔH_i and initiates GB embrittlement at room temperature [152]. The solute decoration at RHAGBs, however, drastically decreases once austenitic transformation takes place, increasing the cohesive strength of the GB [152]. The previously indicated model has also been used to steels based on Fe-9Mn (wt%) [19], [113], [153], [154]. According to Yoo et al. [155], adding 0.15 at.% Mo increases the HE resistance of a 32MnB5 hot-stamping steel. This was explained by the decrease in H diffusivity caused by Mo [155]. Additionally, Mo has been shown to increase GB cohesive strength and decrease strain localization along austenite RHAGBs, which results in a change from an intergranular to a transgranular mode of fracture propagation [155]. According to reports, segregation of P (at ferrite RHAGBs) significantly lowers the cohesive strength of GB in the context of Fe-1.62Mn-0.18Si (wt.%) ferritic steel [111]. On the other hand, it has been noted that the presence of C (at RHAGBs) promotes strengthening at GBs [111].

3. Future directions

To address all five macroscopic and three microscopic DOFs (related to GBs) is a significant issue for GB research. Despite the fact that the 3D EBSD technique (suggested in Ref. [156]) handles all five DOFs (in a GB), it has yet not been possible experimentally to address the three microscopic DOFs. Additionally, the 3D EBSD approach requires an extra FIB setup in a SEM and is quite time-consuming. Because of this, this characterization cannot be carried out in a standard SEM, unlike conventional 2D-EBSD approach. Limitations in linking the GB structure and solute decorating with their overall impact on the mechanical performance of the material result from the inability to address the eight DOFs. However, the only information necessary when using GB segregation information to minimise the overall grain size is the degree of GB segregation. A comprehensive 5D GB analysis is not necessary in this case since information regarding the GB plane may be disregarded [2]. Additionally, 3D-EBSD employs serial sectioning, making it potentially harmful [156], [157]. In other words, since the region being studied is already lost during 3D-EBSD mapping and is not accessible for APT analysis, it is not possible to develop a correlative 3D-EBSD-APT methodology to obtain both structural and chemical information from the same region in a microstructure [157]. However, there is

currently a lack of knowledge on how the density of segregating solute species and the dislocation density (at pile-ups near GBs) affect the cohesive strength of GBs. This might be attributable to the multiple experimental difficulties involved in figuring out how a GB interacts with the species of decorative solute. To overcome the aforementioned issue, it may be possible to employ the correlative approach of microstructural characterisation (described in section 3.2.2) in conjunction with the relevant theoretical studies.

4. Summary and conclusions

There are a number of phenomena that are typically caused by solute decorating at internal interfaces, such as strain-induced phase change (at the internal interfaces), bulk phase creation, phase reversion, and intergranular embrittlement. From a metallurgical perspective, interfacial segregation can be used to manipulate internal interfaces chemically and structurally. The main goal of the aforementioned modification is to improve steels' general mechanical performance. Nevertheless, this is also an area where correlative microscopy may be used in conjunction with the relevant theoretical assessments as a design tool towards manufacturing high-performance steels.

Acknowledgement

The author hereby declares that the review article is solely authored by him. No external assistance of any kind has been received for the article.

References

[1] M. P. Seah, "Interface adsorption, embrittlement and fracture in metallurgy. A review," *Surface Science*, vol. 53, no. 1. pp. 168–212, 1975. doi: 10.1016/0039-6028(75)90124-7.

[2] D. Raabe *et al.*, "Grain boundary segregation engineering in metallic alloys: A pathway to the design of interfaces," *Current Opinion in Solid State and Materials Science*, vol. 18, no. 4. Elsevier Ltd, pp. 253–261, Aug. 01, 2014. doi: 10.1016/j.cossms.2014.06.002.

[3] C.-S. Kim, Y. Hu, G. S. Rohrer, and V. Randle, "Five-parameter grain boundary distribution in grain boundary engineered brass," *Elsevier*, doi: 10.1016/j.scriptamat.2004.11.025.

[4] C. A. Schuh and K. Lu, "Stability of nanocrystalline metals: The role of grain-boundary chemistry and structure," *MRS Bulletin*, vol. 46, no. 3, pp. 225–235, Mar. 2021, doi: 10.1557/s43577-021-00055-x.

[5] D. Raabe *et al.*, "Current Challenges and Opportunities in Microstructure-Related Properties of Advanced High-Strength Steels," *Metallurgical and Materials Transactions A: Physical Metallurgy and Materials Science*, vol. 51, no. 11, pp. 5517–5586, Nov. 2020, doi: 10.1007/s11661-020-05947-2.

[6] E. D. Hondros and C. Lea, “Grain boundary microchemistry and stress-corrosion failure of mild steel,” *Nature*, vol. 289, no. 5799, pp. 663–665, 1981, doi: 10.1038/289663a0.

[7] D. E. Spearot and M. D. Sangid, “Insights on slip transmission at grain boundaries from atomistic simulations,” *Current Opinion in Solid State and Materials Science*, vol. 18, no. 4. Elsevier Ltd, pp. 188–195, Aug. 01, 2014. doi: 10.1016/j.cossms.2014.04.001.

[8] D. Brandon, “25 Year Perspective Defining grain boundaries: An historical perspective the development and limitations of coincident site lattice models,” *Materials Science and Technology*, vol. 26, no. 7. pp. 762–773, Jul. 01, 2010. doi: 10.1179/026708310X12635619987989.

[9] D. G. Brandon, “The structure of high-angle grain boundaries,” *Acta Metallurgica*, vol. 14, no. 11, pp. 1479–1484, 1966, doi: 10.1016/0001-6160(66)90168-4.

[10] E. D. Hondros, “Rule for surface enrichment in solutions,” *Scripta Metallurgica*, vol. 14, no. 3, pp. 345–348, 1980, doi: 10.1016/0036-9748(80)90357-9.

[11] A. P. Sutton, R. W. Balluffi, and V. Vitek, “On intrinsic secondary grain boundary dislocation arrays in high angle symmetrical tilt grain boundaries,” *Scripta Metallurgica*, vol. 15, no. 9, pp. 989–994, 1981, doi: 10.1016/0036-9748(81)90240-4.

[12] H. Grimmer, “Coincidence-site lattices,” *Acta Crystallographica Section A*, vol. 32, no. 5, pp. 783–785, Sep. 1976, doi: 10.1107/S056773947601231X.

[13] F. C. FRANK, “Grain Boundaries in Metals,” *Nature*, vol. 181, no. 4614, pp. 976–977, Apr. 1958, doi: 10.1038/181976b0.

[14] M. E. Glicksman and R. A. Masumura, “GRAIN BOUNDARY STRUCTURE AND ENERGETICS.,” *Metall Trans A*, vol. 8 A, no. 9, pp. 1373–1382, 1977, doi: 10.1007/BF02642851.

[15] V. Y. Gertsman, A. P. Zhilyaev, and J. A. Szpunar, “Grain boundary misorientation distributions in monoclinic zirconia,” *Modelling and Simulation in Materials Science and Engineering*, vol. 5, no. 1, pp. 35–52, Jan. 1997, doi: 10.1088/0965-0393/5/1/003.

[16] J. M. Howe, *Solid-Liquid and Solid-Solid Interfaces*. 1997. Accessed: Jun. 28, 2021. [Online]. Available: https://www.wiley.com/en-us/9780471138303

[17] F. Weinberg, “Grain boundaries in metals,” *Progress in Metal Physics*, vol. 8, no. C, pp. 105–146, Jan. 1959, doi: 10.1016/0502-8205(59)90014-0.

[18] D. Mclean and A. Maradudin, “Grain Boundaries in Metals,” *Citation: Physics Today*, vol. 11, p. 35, 1958, doi: 10.1063/1.3062658.

[19] Saha, M., 2022. Grain boundary segregation in steels: Towards engineering the design of internal interfaces. *arXiv preprint arXiv:2202.12971*.

[20] A. P. Sutton and R. W. Balluffi, “Overview no. 61 On geometric criteria for low interfacial energy,” *Acta Metallurgica*, vol. 35, no. 9, pp. 2177–2201, 1987, doi: 10.1016/0001-6160(87)90067-8.

[21] W. T. Read and W. Shockley, “Dislocation models of crystal grain boundaries,” *Physical Review*, vol. 78, no. 3, pp. 275–289, 1950, doi: 10.1103/PhysRev.78.275.

[22] J. W. Cahn, Y. Mishin, and A. Suzuki, “Duality of dislocation content of grain boundaries,” *Philosophical Magazine*, vol. 86, no. 25–26, pp. 3965–3980, Sep. 2006, doi: 10.1080/14786430500536909.

[23] A. H. Cottrell, “Unified theory of effects of segregated interstitials on grain boundary cohesion,” *Materials Science and Technology (United Kingdom)*, vol. 6, no. 9, pp. 806–810, 1990, doi: 10.1179/mst.1990.6.9.806.

[24] A. Kelly, W. R. Tyson, and A. H. Cottrell, “Ductile and brittle crystals,” *Philosophical Magazine*, vol. 15, no. 135, pp. 567–586, 1967, doi: 10.1080/14786436708220903.

[25] W. T. Geng, A. J. Freeman, and G. B. Olson, “Influence of alloying additions on the impurity induced grain boundary embrittlement,” *Solid State Communications*, vol. 119, no. 10–11, pp. 585–590, 2001, doi: 10.1016/S0038-1098(01)00298-8.

[26] W. T. Geng, A. J. Freeman, and G. B. Olson, “Influence of alloying additions on grain boundary cohesion of transition metals: First-principles determination and its phenomenological extension,” *Physical Review B - Condensed Matter and Materials Physics*, vol. 63, no. 16, pp. 1–9, 2001, doi: 10.1103/PhysRevB.63.165415.

[27] W. T. Geng, A. J. Freeman, R. Wu, and G. B. Olson, “Effect of Mo and Pd on the grain-boundary cohesion of Fe,” *Physical Review B - Condensed Matter and Materials Physics*, vol. 62, no. 10, pp. 6208–6214, 2000, doi: 10.1103/PhysRevB.62.6208.

[28] H. K. Birnbaum and P. Sofronis, “Hydrogen-enhanced localized plasticity-a mechanism for hydrogen-related fracture,” *Materials Science and Engineering A*, vol. 176, no. 1–2, pp. 191–202, Mar. 1994, doi: 10.1016/0921-5093(94)90975-X.

[29] B. A. Szost, R. H. Vegter, and P. E. J. Rivera-Díaz-Del-Castillo, “Hydrogen-trapping mechanisms in nanostructured steels,” *Metallurgical and Materials Transactions A: Physical Metallurgy and Materials Science*, vol. 44, no. 10, pp. 4542–4550, Oct. 2013, doi: 10.1007/s11661-013-1795-7.

[30] K. Takai, H. Shoda, H. Suzuki, and M. Nagumo, “Lattice defects dominating hydrogen-related failure of metals,” *Acta Materialia*, vol. 56, no. 18, pp. 5158–5167, Oct. 2008, doi: 10.1016/j.actamat.2008.06.031.

[31] Y. Toji, H. Matsuda, M. Herbig, P. P. Choi, and D. Raabe, “Atomic-scale analysis of carbon partitioning between martensite and austenite by atom probe tomography and correlative transmission electron microscopy,” *Acta Materialia*, vol. 65, pp. 215–228, Feb. 2014, doi: 10.1016/j.actamat.2013.10.064.

[32] T. Frolov and Y. Mishin, “Thermodynamics of coherent interfaces under mechanical stresses. II. Application to atomistic simulation of grain boundaries,” *Physical Review B - Condensed Matter and Materials Physics*, vol. 85, no. 22, 2012, doi: 10.1103/PhysRevB.85.224107.

[33] Z. T. Trautt and Y. Mishin, “Grain boundary migration and grain rotation studied by molecular dynamics,” *Acta Materialia*, vol. 60, no. 5, pp. 2407–2424, 2012, doi: 10.1016/j.actamat.2012.01.008.

[34] M. Winning and A. D. Rollett, “Transition between low and high angle grain boundaries,” *Acta Materialia*, vol. 53, no. 10, pp. 2901–2907, Jun. 2005, doi: 10.1016/j.actamat.2005.03.005.

[35] A. D. Rollett and P. N. Kalu, “Grain Boundary Properties : Energy,” *Revue de Métallurgie*, pp. 1–82, 2008.

[36] A. D. Rollett, D. J. Srolovitz, and A. Karma, “Editorial: Microstructural evolution based on fundamental interracial properties,” *Interface Science*, vol. 10, no. 2–3. p. 119, Jul. 2002. doi: 10.1023/A:1015809611353.

[37] S. Mandal, B. T. Gockel, and A. D. Rollett, “Application of canonical correlation analysis to a sensitivity study of constitutive model parameter fitting,” *Materials and Design*, vol. 132, pp. 30–43, Oct. 2017, doi: 10.1016/j.matdes.2017.06.050.

[38] N. Bandyopadhyay, C. L. Briant, and E. L. Hall, “Carbide precipitation, grain boundary segregation, and temper embrittlement in NiCrMoV rotor steels,” *Metallurgical Transactions A 1985 16:5*, vol. 16, no. 5, pp. 721–737, May 1985, doi: 10.1007/BF02814824.

[39] C. L. Brunt, “Sources of variability in grain boundary segregation,” *Acta Metallurgica*, vol. 31, no. 2, pp. 257–266, Feb. 1983, doi: 10.1016/0001-6160(83)90102-5.

[40] G. M. Carinci, “Grain boundary segregation of boron in an austenitic stainless steel,” *Applied Surface Science*, vol. 76–77, no. C, pp. 266–271, Mar. 1994, doi: 10.1016/0169-4332(94)90353-0.

[41] S. H. Song, J. Wu, L. Q. Weng, and Z. X. Yuan, “Fractographic changes caused by phosphorus grain boundary segregation for a low alloy structural steel,” *Materials Science and Engineering: A*, vol. 497, no. 1–2, pp. 524–527, Dec. 2008, doi: 10.1016/J.MSEA.2008.07.036.

[42] X. M. Chen, S. H. Song, L. Q. Weng, and S. J. Liu, “Solute grain boundary segregation during high temperature plastic deformation in a Cr–Mo low alloy steel,” *Materials Science and Engineering: A*, vol. 528, no. 25–26, pp. 7663–7668, Sep. 2011, doi: 10.1016/J.MSEA.2011.06.084.

[43] C. L. Briant and S. K. Banerji, “Intergranular failure in steel: the role of grain-boundary composition,” *International Materials Reviews*, vol. 23, no. 1, pp. 164–199, Jan. 2012, doi: 10.1179/095066078790136652.

[44] X. Tingdong, “Non-equilibrium grain-boundary segregation kinetics,” *Journal of Materials Science 1987 22:1*, vol. 22, no. 1, pp. 337–345, Jan. 1987, doi: 10.1007/BF01160590.

[45] T. Xu and S. Song, “A kinetic model of non-equilibrium grain-boundary segregation,” *Acta Metallurgica*, vol. 37, no. 9, pp. 2499–2506, Sep. 1989, doi: 10.1016/0001-6160(89)90048-5.

[46] X. Sauvage, A. Ganeev, Y. Ivanisenko, N. Enikeev, M. Murashkin, and R. Valiev, “Grain Boundary Segregation in UFG Alloys Processed by Severe Plastic Deformation,” *Advanced Engineering Materials*, vol. 14, no. 11, pp. 968–974, Nov. 2012, doi: 10.1002/ADEM.201200060.

[47] M. P. Seah, “Segregation and the Strength of Grain Boundaries.,” *Proc R Soc Lond Ser A*, vol. 349, no. 1659, pp. 535–554, 1976, doi: 10.1098/rspa.1976.0088.

[48] M. P. Seah, "Adsorption-induced interface decohesion," *Acta Metallurgica*, vol. 28, no. 7, pp. 955–962, Jul. 1980, doi: 10.1016/0001-6160(80)90112-1.

[49] D. Raabe *et al.*, "Metallic composites processed via extreme deformation: Toward the limits of strength in bulk materials," *MRS Bulletin*, vol. 35, no. 12, pp. 982–991, Jan. 2010, doi: 10.1557/mrs2010.703.

[50] P. Lejček, "Effect of Variables on Equilibrium Grain Boundary Segregation," in *Springer Series in Materials Science*, 2010. doi: 10.1007/978-3-642-12505-8_5.

[51] Y. Ohmori and T. Kunitake, "Effects of austenite grain size and grain boundary segregation of impurity atoms on high temperature ductility," *Metal Science*, vol. 17, no. 7, pp. 325–332, Jul. 1983, doi: 10.1179/030634583790420781.

[52] P. Lejček, "On the thermodynamic description of grain boundary segregation in polycrystals," *Materials Science and Engineering A*, vol. 185, no. 1–2, pp. 109–114, Sep. 1994, doi: 10.1016/0921-5093(94)90933-4.

[53] L. Karlsson and H. Nordén, "Overview no. 63 Non-equilibrium grain boundary segregation of boron in austenitic stainless steel-II. Fine scale segregation behaviour," *Acta Metallurgica*, vol. 36, no. 1, pp. 13–24, Jan. 1988, doi: 10.1016/0001-6160(88)90024-7.

[54] S. H. Song, H. Zhuang, J. Wu, L. Q. Weng, Z. X. Yuan, and T. H. Xi, "Dependence of ductile-to-brittle transition temperature on phosphorus grain boundary segregation for a 2.25Cr1Mo steel," *Materials Science and Engineering: A*, vol. 486, no. 1–2, pp. 433–438, Jul. 2008, doi: 10.1016/J.MSEA.2007.09.032.

[55] M. A. Tschopp and D. L. McDowell, "Structures and energies of ∑3 asymmetric tilt grain boundaries in copper and aluminium," *Philosophical Magazine*, vol. 87, no. 22, pp. 3147–3173, Aug. 2007, doi: 10.1080/14786430701255895.

[56] M. A. Tschopp, K. N. Solanki, F. Gao, X. Sun, M. A. Khaleel, and M. F. Horstemeyer, "Probing grain boundary sink strength at the nanoscale: Energetics and length scales of vacancy and interstitial absorption by grain boundaries in α-Fe," *Physical Review B - Condensed Matter and Materials Physics*, vol. 85, no. 6, Feb. 2012, doi: 10.1103/PhysRevB.85.064108.

[57] M. A. V. Chapman and R. G. Faulkner, "Computer modelling of grain boundary segregation," *Acta Metallurgica*, vol. 31, no. 5, pp. 677–689, May 1983, doi: 10.1016/0001-6160(83)90083-4.

[58] B. W. Krakauer and D. N. Seidman, "Absolute atomic-scale measurements of the Gibbsian interfacial excess of solute at internal interfaces," *Physical Review B*, vol. 48, no. 9, pp. 6724–6727, 1993, doi: 10.1103/PhysRevB.48.6724.

[59] E. D. Hondros and D. McLean, "Cohesion margin of copper," *Philosophical Magazine*, vol. 29, no. 4, pp. 771–795, 1974, doi: 10.1080/14786437408222070.

[60] I. Langmuir, "The adsorption of gases on plane surfaces of glass, mica and platinum," *Journal of the American Chemical Society*, vol. 40, no. 9, pp. 1361–1403, Sep. 1918, doi: 10.1021/ja02242a004.

[61] P. Lejček, M. Šob, V. Paidar, and V. Vitek, “Why calculated energies of grain boundary segregation are unreliable when segregant solubility is low,” *Scripta Materialia*, vol. 68, no. 8, pp. 547–550, Apr. 2013, doi: 10.1016/j.scriptamat.2012.11.019.

[62] P. Lejček and S. Hofmann, “Entropy-dominated grain boundary segregation,” *Journal of Materials Science*, vol. 56, no. 12, pp. 7464–7473, Apr. 2021, doi: 10.1007/s10853-021-05800-w.

[63] P. Lejček, S. Hofmann, M. Všianská, and M. Šob, “Entropy matters in grain boundary segregation,” *Acta Materialia*, vol. 206, p. 116597, Mar. 2021, doi: 10.1016/j.actamat.2020.116597.

[64] R. H. Ewing, “An analytical approach to interfacial entropy,” *Acta Metallurgica*, vol. 19, no. 12, pp. 1359–1362, 1971, doi: 10.1016/0001-6160(71)90073-3.

[65] P. Lejček and S. Hofmann, “Thermodynamics and structural aspects of grain boundary segregation,” *Critical Reviews in Solid State and Materials Sciences*, vol. 20, no. 1, pp. 1–85, 1995, doi: 10.1080/10408439508243544.

[66] P. Lejček and S. Hofmann, “Grain boundary segregation diagrams of α-iron,” *Interface Science*, vol. 1, no. 2, pp. 163–174, 1993, doi: 10.1007/BF00203606.

[67] P. Lejcek and S. Hofmann, “Thermodynamics of grain boundary segregation and applications to anisotropy, compensation effect and prediction,” *Critical Reviews in Solid State and Materials Sciences*, vol. 33, no. 2, pp. 133–163, Apr. 2008, doi: 10.1080/10408430801907649.

[68] P. Lejček, S. Hofmann, and V. Paidar, “The significance of entropy in grain boundary segregation,” *Materials*, vol. 12, no. 3, pp. 1–9, 2019, doi: 10.3390/ma12030492.

[69] P. Lejček, “Enthalpy-entropy compensation effect in grain boundary phenomena,” *Zeitschrift fuer Metallkunde/Materials Research and Advanced Techniques*, vol. 96, no. 10, pp. 1129–1133, 2005, doi: 10.3139/146.101151.

[70] P. Lejček, “Characterization of grain boundary segregation in an Fe-Si alloy,” *Analytica Chimica Acta*, vol. 297, no. 1–2, pp. 165–178, Oct. 1994, doi: 10.1016/0003-2670(93)E0388-N.

[71] P. Lejček, R. Konečná, and J. Janovec, “Solute segregation to ferrite grain boundaries in nodular cast iron: Experiment and prediction,” *Surface and Interface Analysis*, vol. 40, no. 3–4, pp. 503–506, 2008, doi: 10.1002/sia.2659.

[72] P. Lejček, M. Všianská, and M. Šob, “Recent trends and open questions in grain boundary segregation,” *Journal of Materials Research*, vol. 33, no. 18, pp. 2647–2660, Sep. 2018, doi: 10.1557/jmr.2018.230.

[73] P. Lejček, J. Adámek, and S. Hofmann, “Anisotropy of grain boundary segregation in $\Sigma = 5$ bicrystals of α-iron,” *Surface Science*, vol. 264, no. 3, pp. 449–454, Mar. 1992, doi: 10.1016/0039-6028(92)90201-G.

[74] P. Lejček, S. Hofmann, and J. Janovec, “Prediction of enthalpy and entropy of solute segregation at individual grain boundaries of α-iron and ferrite steels,” *Materials Science and Engineering A*, vol. 462, no. 1–2, pp. 76–85, Jul. 2007, doi: 10.1016/j.msea.2006.02.463.

[75] P. Lejček, M. Šob, and V. Paidar, “Interfacial segregation and grain boundary embrittlement: An overview and critical assessment of experimental data and calculated results,” *Progress in Materials Science*, vol. 87. 2017. doi: 10.1016/j.pmatsci.2016.11.001.

[76] S. Hofmann and P. Lejček, “Correlation between segregation enthalpy, solid solubility and interplanar spacing of Σ=5 tilt grain boundaries in α-iron,” *Scripta Metallurgica et Materiala*, vol. 25, no. 10, pp. 2259–2262, 1991, doi: 10.1016/0956-716X(91)90011-O.

[77] P. Lejček and S. Hofmann, “Grain boundary segregation diagrams of α-iron,” *Interface Science*, vol. 1, no. 2, pp. 163–174, 1993, doi: 10.1007/BF00203606.

[78] M. Guttmann, “Interfacial Segregation in Multicomponent Systems,” in *Atomistics of Fracture*, Boston, MA: Springer US, 1983, pp. 465–494. doi: 10.1007/978-1-4613-3500-9_17.

[79] M. Guttmann, “Grain boundary segregation, two dimensional compound formation, and precipitation,” *Metallurgical Transactions A*, vol. 8, no. 9, pp. 1383–1401, Sep. 1977, doi: 10.1007/BF02642852.

[80] M. Guttmann, “Equilibrium segregation in a ternary solution: A model for temper embrittlement,” *Surface Science*, vol. 53, no. 1, pp. 213–227, 1975, doi: 10.1016/0039-6028(75)90125-9.

[81] M. Guttmann, “Interfacial Segregation in Multicomponent Systems,” in *Atomistics of Fracture*, Boston, MA: Springer US, 1983, pp. 465–494. doi: 10.1007/978-1-4613-3500-9_17.

[82] P. Wynblatt and D. Chatain, “Anisotropy of segregation at grain boundaries and surfaces,” *Metallurgical and Materials Transactions A: Physical Metallurgy and Materials Science*, vol. 37, no. 9. pp. 2595–2620, Sep. 2006. doi: 10.1007/BF02586096.

[83] M. Daly *et al.*, “A multi-scale correlative investigation of ductile fracture,” *Acta Materialia*, vol. 130, pp. 56–68, May 2017, doi: 10.1016/j.actamat.2017.03.028.

[84] S. E. Hopkin, M. Danaie, G. Guetard, P. Rivera-Diaz-del-Castillo, P. A. J. Bagot, and M. P. Moody, “Correlative atomic scale characterisation of secondary carbides in M50 bearing steel,” *Philosophical Magazine*, vol. 98, no. 9, pp. 766–782, Mar. 2018, doi: 10.1080/14786435.2017.1410290.

[85] T. Schwarz, G. Stechmann, B. Gault, O. Cojocaru-Mirédin, R. Wuerz, and D. Raabe, “Correlative transmission Kikuchi diffraction and atom probe tomography study of Cu(In,Ga)Se2 grain boundaries,” *Progress in Photovoltaics: Research and Applications*, vol. 26, no. 3, pp. 196–204, Mar. 2018, doi: 10.1002/pip.2966.

[86] M. Herbig, D. Raabe, Y. J. Li, P. Choi, S. Zaefferer, and S. Goto, “Atomic-Scale Quantification of Grain Boundary Segregation in Nanocrystalline Material,” *APS*, vol. 112, no. 12, Dec. 2014, doi: 10.1103/PhysRevLett.112.126103.

[87] Y. J. Li, A. Kostka, A. Savan, and A. Ludwig, “Correlative chemical and structural investigations of accelerated phase evolution in a nanocrystalline high entropy alloy,” *Scripta Materialia*, vol. 183, pp. 122–126, Jul. 2020, doi: 10.1016/j.scriptamat.2020.03.016.

[88] L. Yao, S. P. Ringer, J. M. Cairney, and M. K. Miller, “The anatomy of grain boundaries: Their structure and atomic-level solute distribution,” *Scripta Materialia*, vol. 69, no. 8, pp. 622–625, Oct. 2013, doi: 10.1016/j.scriptamat.2013.07.013.

[89] B. Gault, M. P. Moody, J. M. Cairney, and S. P. Ringer, “Atom Atom probe probe crystallography,” *Materials Today*, vol. 15, no. 9, pp. 378–386, 2012, doi: 10.1016/S1369-7021(12)70164-5.

[90] B. Gault, M. P. Moody, J. M. Cairney, and S. P. Ringer, “Specimen Preparation,” in *Springer Series in Materials Science*, vol. 160, Springer Science and Business Media Deutschland GmbH, 2012, pp. 71–110. doi: 10.1007/978-1-4614-3436-8_4.

[91] D. J. Larson, B. P. Geiser, T. J. Prosa, and T. F. Kelly, “Atom Probe Tomography Spatial Reconstruction : Current Status and Future Directions,” *Current Opinion in Solid State and Materials Science*, vol. 39, pp. 740–741, 2012.

[92] A. v. Ceguerra *et al.*, “The rise of computational techniques in atom probe microscopy,” *Current Opinion in Solid State and Materials Science*. 2013. doi: 10.1016/j.cossms.2013.09.006.

[93] O. Dmitrieva *et al.*, “Chemical gradients across phase boundaries between martensite and austenite in steel studied by atom probe tomography and simulation,” *Acta Materialia*, vol. 59, no. 1, pp. 364–374, Jan. 2011, doi: 10.1016/j.actamat.2010.09.042.

[94] H. J. Grabke, R. Möller, H. Erhart, and S. S. Brenner, “Effects of the alloying elements Ti, Nb, Mo and V on the grain boundary segregation of P in iron and steels,” *Surface and Interface Analysis*, vol. 10, no. 4, pp. 202–209, Apr. 1987, doi: 10.1002/sia.740100405.

[95] F. Christien, R. le Gall, and G. Saindrenan, “Phosphorus grain boundary segregation in steel 17-4PH,” *Scripta Materialia*, vol. 48, no. 1, pp. 11–16, Jan. 2003, doi: 10.1016/S1359-6462(02)00309-3.

[96] J. Takahashi, K. Kawakami, K. Ushioda, S. Takaki, N. Nakata, and T. Tsuchiyama, “Quantitative analysis of grain boundaries in carbon- and nitrogen-added ferritic steels by atom probe tomography,” *Scripta Materialia*, vol. 66, no. 5, pp. 207–210, Mar. 2012, doi: 10.1016/j.scriptamat.2011.10.026.

[97] G. da Rosa *et al.*, “Grain-boundary segregation of boron in high-strength steel studied by nano-SIMS and atom probe tomography,” *Acta Materialia*, vol. 182, pp. 226–234, Jan. 2020, doi: 10.1016/j.actamat.2019.10.029.

[98] Z. N. Abdellah, R. Chegroune, M. Keddam, B. Bouarour, L. Haddour, and A. Elias, “The phase stability in the Fe-B binary system: Comparison between the interstitial and substitutional models,” *Defect and Diffusion Forum*, vol. 322, pp. 1–9, Mar. 2012, doi: 10.4028/www.scientific.net/DDF.322.1.

[99] J. MORRAL, M. JE, and J. W. JR, “THE BINDING ENERGY OF BORON TO AUSTENITE GRAIN BOUNDARIES AS CALCULATED FROM AUTORADIOGRAPHY,” *THE BINDING ENERGY OF BORON TO AUSTENITE GRAIN BOUNDARIES AS CALCULATED FROM AUTORADIOGRAPHY*, 1980.

[100] R. G. Faulkner, “Radiation-induced grain boundary segregation in nuclear reactor steels,” *Journal of Nuclear Materials*, vol. 251, pp. 269–275, 1997, doi: 10.1016/S0022-3115(97)00248-1.

[101] S. v. Fedotova, E. A. Kuleshova, D. A. Maltsev, and M. A. Saltykov, “Complex study of grain boundary segregation in long-term irradiated reactor pressure vessel steels,” *Journal of Nuclear Materials*, vol. 528, p. 151865, Jan. 2020, doi: 10.1016/j.jnucmat.2019.151865.

[102] K. Hata, H. Takamizawa, T. Hojo, K. Ebihara, Y. Nishiyama, and Y. Nagai, “Grain-boundary phosphorus segregation in highly neutron-irradiated reactor pressure vessel steels and its effect on irradiation embrittlement,” *Journal of Nuclear Materials*, vol. 543, p. 152564, Jan. 2021, doi: 10.1016/j.jnucmat.2020.152564.

[103] T. Toyama *et al.*, “Grain boundary segregation in neutron-irradiated 304 stainless steel studied by atom probe tomography,” in *Journal of Nuclear Materials*, Jun. 2012, vol. 425, no. 1–3, pp. 71–75. doi: 10.1016/j.jnucmat.2011.11.072.

[104] E. A. Kenik, T. Inazumi, and G. E. C. Bell, “Radiation-induced grain boundary segregation and sensitization of a neutron-irradiated austenitic stainless steel,” *Journal of Nuclear Materials*, vol. 183, no. 3, pp. 145–153, Aug. 1991, doi: 10.1016/0022-3115(91)90482-M.

[105] G. Shigesato, T. Fujishiro, and T. Hara, “Boron segregation to austenite grain boundary in low alloy steel measured by aberration corrected STEM-EELS,” *Materials Science and Engineering A*, vol. 556, pp. 358–365, Oct. 2012, doi: 10.1016/j.msea.2012.06.099.

[106] Y. Ma *et al.*, “Phase boundary segregation-induced strengthening and discontinuous yielding in ultrafine-grained duplex medium-Mn steels,” *Acta Materialia*, vol. 200, pp. 389–403, Nov. 2020, doi: 10.1016/j.actamat.2020.09.007.

[107] T. Frolov, “Effect of interfacial structural phase transitions on the coupled motion of grain boundaries: A molecular dynamics study,” *Applied Physics Letters*, vol. 104, no. 21, p. 211905, May 2014, doi: 10.1063/1.4880715.

[108] G. Gottstein, L. S. Shvindlerman, and B. Zhao, “Thermodynamics and kinetics of grain boundary triple junctions in metals: Recent developments,” *Scripta Materialia*, vol. 62, no. 12, pp. 914–917, 2010, doi: 10.1016/j.scriptamat.2010.03.017.

[109] G. Gottstein, D. A. Molodov, and L. S. Shvindlerman, “Grain boundary migration in metals: recent developments,” *Interface Science*, vol. 6, no. 1–2, pp. 7–22, Feb. 1998, doi: 10.1023/A:1008641617937.

[110] M. M. Abramova *et al.*, “Grain boundary segregation induced strengthening of an ultrafine-grained austenitic stainless steel,” *Materials Letters*, vol. 136, pp. 349–352, Dec. 2014, doi: 10.1016/j.matlet.2014.07.188.

[111] J. C. Han, J. B. Seol, M. Jafari, J. E. Kim, S. J. Seo, and C. G. Park, “Competitive grain boundary segregation of phosphorus and carbon governs delamination crack in a ferritic steel,” *Materials Characterization*, vol. 145, pp. 454–460, Nov. 2018, doi: 10.1016/j.matchar.2018.08.060.

[112] M. Kuzmina, D. Ponge, and D. Raabe, “Grain boundary segregation engineering and austenite reversion turn embrittlement into toughness: Example of a 9 wt.% medium Mn steel,” *Acta Materialia*, vol. 86, pp. 182–192, Mar. 2015, doi: 10.1016/j.actamat.2014.12.021.

[113] J. T. Benzing *et al.*, “Multi-scale characterization of austenite reversion and martensite recovery in a cold-rolled medium-Mn steel,” *Acta Materialia*, vol. 166, pp. 512–530, Mar. 2019, doi: 10.1016/j.actamat.2019.01.003.

[114] A. M. Ravi, A. Kumar, M. Herbig, J. Sietsma, and M. J. Santofimia, “Impact of austenite grain boundaries and ferrite nucleation on bainite formation in steels,” *Acta Materialia*, vol. 188, pp. 424–434, Apr. 2020, doi: 10.1016/j.actamat.2020.01.065.

[115] M. Herbig *et al.*, “Grain boundary segregation in Fe-Mn-C twinning-induced plasticity steels studied by correlative electron backscatter diffraction and atom probe tomography,” *Acta Materialia*, vol. 83, pp. 37–47, Jan. 2015, doi: 10.1016/j.actamat.2014.09.041.

[116] S. Araki, K. Mashima, T. Masumura, T. Tsuchiyama, S. Takaki, and T. Ohmura, “Effect of grain boundary segregation of carbon on critical grain boundary strength of ferritic steel,” *Scripta Materialia*, vol. 169, pp. 38–41, Aug. 2019, doi: 10.1016/j.scriptamat.2019.05.001.

[117] L. Yuan, D. Ponge, J. Wittig, P. Choi, J. A. Jiménez, and D. Raabe, “Nanoscale austenite reversion through partitioning, segregation and kinetic freezing: Example of a ductile 2 GPa Fe-Cr-C steel,” *Acta Materialia*, vol. 60, no. 6–7, pp. 2790–2804, Apr. 2012, doi: 10.1016/j.actamat.2012.01.045.

[118] Y. J. Li *et al.*, “Atomic-scale mechanisms of deformation-induced cementite decomposition in pearlite,” *Acta Materialia*, vol. 59, no. 10, pp. 3965–3977, Jun. 2011, doi: 10.1016/j.actamat.2011.03.022.

[119] Y. J. Li, P. Choi, S. Goto, C. Borchers, D. Raabe, and R. Kirchheim, “Evolution of strength and microstructure during annealing of heavily cold-drawn 6.3 GPa hypereutectoid pearlitic steel wire,” *Acta Materialia*, vol. 60, no. 9, pp. 4005–4016, May 2012, doi: 10.1016/j.actamat.2012.03.006.

[120] Y. J. Lia *et al.*, “Atom probe tomography characterization of heavily cold drawn pearlitic steel wire,” *Ultramicroscopy*, vol. 111, no. 6, pp. 628–632, May 2011, doi: 10.1016/j.ultramic.2010.11.010.

[121] Y. S. Chen *et al.*, “Direct observation of individual hydrogen atoms at trapping sites in a ferritic steel,” *Science*, vol. 355, no. 6330, pp. 1196–1199, Mar. 2017, doi: 10.1126/science.aal2418.

[122] J. Cairney, “Atoms on the move - Finding the hydrogen,” *Science*, vol. 355, no. 6330. American Association for the Advancement of Science, pp. 1128–1129, Mar. 17, 2017. doi: 10.1126/science.aam8616.

[123] I. M. Robertson *et al.*, “Hydrogen Embrittlement Understood,” *Metallurgical and Materials Transactions B: Process Metallurgy and Materials Processing Science*, vol. 46, no. 3, pp. 1085–1103, Jun. 2015, doi: 10.1007/s11663-015-0325-y.

[124] Y. S. Chen *et al.*, “Observation of hydrogen trapping at dislocations, grain boundaries, and precipitates,” *Science*, vol. 367, no. 6474, pp. 171–175, Jan. 2020, doi: 10.1126/science.aaz0122.

[125] M. Koyama, E. Akiyama, and K. Tsuzaki, “Effect of hydrogen content on the embrittlement in a Fe-Mn-C twinning-induced plasticity steel,” *Corrosion Science*, vol. 59, pp. 277–281, Jun. 2012, doi: 10.1016/j.corsci.2012.03.009.

[126] I. R. Souza Filho *et al.*, “Sustainable steel through hydrogen plasma reduction of iron ore: Process, kinetics, microstructure, chemistry,” *Acta Materialia*, vol. 213, p. 116971, Jul. 2021, doi: 10.1016/j.actamat.2021.116971.

[127] S. H. Kim *et al.*, “Influence of microstructure and atomic-scale chemistry on the direct reduction of iron ore with hydrogen at 700°C,” *Acta Materialia*, vol. 212, p. 116933, Jun. 2021, doi: 10.1016/j.actamat.2021.116933.

[128] D. Raabe, C. C. Tasan, and E. A. Olivetti, “Strategies for improving the sustainability of structural metals,” *Nature*, vol. 575, no. 7781. Nature Publishing Group, pp. 64–74, Nov. 07, 2019. doi: 10.1038/s41586-019-1702-5.

[129] M. P. Phaniraj, H. J. Kim, J. Y. Suh, J. H. Shim, S. J. Park, and T. H. Lee, “Hydrogen embrittlement in high interstitial alloyed 18Cr10Mn austenitic stainless steels,” *International Journal of Hydrogen Energy*, vol. 40, no. 39, pp. 13635–13642, Oct. 2015, doi: 10.1016/j.ijhydene.2015.07.163.

[130] D. Raabe, D. Ponge, O. Dmitrieva, and B. Sander, “Nanoprecipitate-hardened 1.5 GPa steels with unexpected high ductility,” *Scripta Materialia*, vol. 60, no. 12, pp. 1141–1144, Jun. 2009, doi: 10.1016/j.scriptamat.2009.02.062.

[131] B. C. Cameron, M. Koyama, and C. C. Tasan, “Phase Stability Effects on Hydrogen Embrittlement Resistance in Martensite–Reverted Austenite Steels,” *Metallurgical and Materials Transactions A: Physical Metallurgy and Materials Science*, vol. 50, no. 1, pp. 29–34, Jan. 2019, doi: 10.1007/s11661-018-4948-x.

[132] Y. S. Chun, J. S. Kim, K. T. Park, Y. K. Lee, and C. S. Lee, “Role of e{open} martensite in tensile properties and hydrogen degradation of high-Mn steels,” *Materials Science and Engineering A*, vol. 533, pp. 87–95, Jan. 2012, doi: 10.1016/j.msea.2011.11.039.

[133] D. Raabe, D. Ponge, O. Dmitrieva, and B. Sander, “Designing ultrahigh strength steels with good ductility by combining transformation induced plasticity and martensite aging,” *Advanced Engineering Materials*, vol. 11, no. 7, pp. 547–555, Jul. 2009, doi: 10.1002/adem.200900061.

[134] G. B. Olson and M. Cohen, “A mechanism for the strain-induced nucleation of martensitic transformations,” *Journal of The Less-Common Metals*, vol. 28, no. 1, pp. 107–118, 1972, doi: 10.1016/0022-5088(72)90173-7.

[135] N. Nakada, T. Tsuchiyama, S. Takaki, and S. Hashizume, “Variant selection of reversed austenite in lath martensite,” *ISIJ International*, vol. 47, no. 10, pp. 1527–1532, 2007, doi: 10.2355/isijinternational.47.1527.

[136] M. R. Hickson, P. J. Hurley, R. K. Gibbs, G. L. Kelly, and P. D. Hodgson, “The Production of Ultrafine Ferrite in Low-Carbon Steel by Strain-Induced Transformation.”

[137] G. Krauss, “Martensite in steel: Strength and structure,” *Materials Science and Engineering A*, vol. 273–275, pp. 40–57, Dec. 1999, doi: 10.1016/s0921-5093(99)00288-9.

[138] M. Kehoe and P. M. Kelly, “The role of carbon in the strength of ferrous martensite,” *Scripta Metallurgica*, vol. 4, no. 6, pp. 473–476, 1970, doi: 10.1016/0036-9748(70)90088-8.

[139] M. P. Seah, “The Theory of Grain Boundary Segregation in Terms of Surface Adsorption Analogues,” vol. 8, no. September, pp. 1363–1371, 1977.

[140] M. Rajagopalan, M. A. Tschopp, and K. N. Solanki, “Grain boundary segregation of interstitial and substitutional impurity atoms in alpha-iron,” *JOM*, vol. 66, no. 1, pp. 129–138, Jan. 2014, doi: 10.1007/s11837-013-0807-9.

[141] M. Wagih and C. A. Schuh, “Spectrum of grain boundary segregation energies in a polycrystal,” *Acta Materialia*, 2019, doi: 10.1016/j.actamat.2019.09.034.

[142] M. A. Gibson and C. A. Schuh, “A survey of ab-initio calculations shows that segregation-induced grain boundary embrittlement is predicted by bond-breaking arguments,” *Scripta Materialia*, vol. 113, pp. 55–58, 2016, doi: 10.1016/j.scriptamat.2015.09.041.

[143] J. R. Trelewicz and C. A. Schuh, “Grain boundary segregation and thermodynamically stable binary nanocrystalline alloys,” *Physical Review B - Condensed Matter and Materials Physics*, vol. 79, no. 9, pp. 1–13, 2009, doi: 10.1103/PhysRevB.79.094112.

[144] M. A. Gibson and C. A. Schuh, “Segregation-induced changes in grain boundary cohesion and embrittlement in binary alloys,” *Acta Materialia*, vol. 95, pp. 145–155, 2015, doi: 10.1016/j.actamat.2015.05.004.

[145] J. P. Hirth and J. R. Rice, “On the thermodynamics of adsorption at interfaces as it influences decohesion,” *Metallurgical Transactions A*, vol. 11, no. 9, pp. 1501–1511, 1980, doi: 10.1007/BF02654514.

[146] J. R. Rice and J. S. Wang, “Embrittlement of interfaces by solute segregation,” *Materials Science and Engineering A*, vol. 107, no. C, pp. 23–40, Jan. 1989, doi: 10.1016/0921-5093(89)90372-9.

[147] M. A. Gibson and C. A. Schuh, “Segregation-induced changes in grain boundary cohesion and embrittlement in binary alloys,” *Acta Materialia*, vol. 95, pp. 145–155, Jun. 2015, doi: 10.1016/j.actamat.2015.05.004.

[148] J. P. Hirth, “Effects of hydrogen on the properties of iron and steel,” *Metallurgical Transactions A*, vol. 11, no. 6, pp. 861–890, Jun. 1980, doi: 10.1007/BF02654700.

[149] M. L. Jokl, V. Vitek, and C. J. McMahon, “MICROSCOPIC THEORY OF BRITTLE FRACTURE IN DEFORMABLE SOLIDS: A RELATION BETWEEN IDEAL WORK TO FRACTURE AND PLASTIC WORK.,” *Acta Metallurgica*, vol. 28, no. 11, pp. 1479–1488, 1980, doi: 10.1016/0001-6160(80)90048-6.

[150] C. J. McMahon, “Brittle fracture of grain boundaries,” *Interface Science*, vol. 12, no. 2–3, pp. 141–146, 2004, doi: 10.1023/B:INTS.0000028644.07075.4e.

[151] J. P. Hirth, R. C. Pond, R. G. Hoagland, X. Y. Liu, and J. Wang, “Interface defects, reference spaces and the Frank–Bilby equation,” *Progress in Materials Science*, vol. 58, no. 5. Elsevier Ltd, pp. 749–823, Jun. 01, 2013. doi: 10.1016/j.pmatsci.2012.10.002.

[152] A. Kwiatkowski da Silva, R. D. Kamachali, D. Ponge, B. Gault, J. Neugebauer, and D. Raabe, “Thermodynamics of grain boundary segregation, interfacial spinodal and their relevance for nucleation during solid-solid phase transitions,” *Acta Materialia*, vol. 168, pp. 109–120, Apr. 2019, doi: 10.1016/j.actamat.2019.02.005.

[153] A. Kwiatkowski da Silva *et al.*, “Confined chemical and structural states at dislocations in Fe-9wt%Mn steels: A correlative TEM-atom probe study combined with multiscale modelling,” *Acta Materialia*, vol. 124, pp. 305–315, Feb. 2017, doi: 10.1016/j.actamat.2016.11.013.

[154] M. Kuzmina, M. Herbig, D. Ponge, S. Sandlöbes, and D. Raabe, “Linear complexions: Confined chemical and structural states at dislocations,” *Science*, vol. 349, no. 6252, pp. 1080–1083, Sep. 2015, doi: 10.1126/science.aab2633.

[155] J. Yoo *et al.*, “Effects of solid solution and grain-boundary segregation of Mo on hydrogen embrittlement in 32MnB5 hot-stamping steels,” *Acta Materialia*, vol. 207, p. 116661, Apr. 2021, doi: 10.1016/j.actamat.2021.116661.

[156] D. J. Rowenhorst, A. Gupta, C. R. Feng, and G. Spanos, “3D Crystallographic and morphological analysis of coarse martensite: Combining EBSD and serial sectioning,” *Scripta Materialia*, vol. 55, no. 1, pp. 11–16, Jul. 2006, doi: 10.1016/J.SCRIPTAMAT.2005.12.061.

[157] M. Calcagnotto, D. Ponge, E. Demir, and D. Raabe, “Orientation gradients and geometrically necessary dislocations in ultrafine grained dual-phase steels studied by 2D and 3D EBSD,” *Materials Science and Engineering: A*, vol. 527, no. 10–11, pp. 2738–2746, Apr. 2010, doi: 10.1016/J.MSEA.2010.01.004.